Local skin inflammation in cutaneous leishmaniasis as a source of variable pharmacokinetics and therapeutic efficacy of liposomal amphotericin B

Gert-Jan Wijnant[1,4], Katrien Van Bocxlaer[1], Amanda Fortes Francisco[2], Vanessa Yardley[1], Andy Harris[3], Mo Alavijeh[3], Sudaxshina Murdan[4] and Simon L. Croft[1]

1. Department of Immunology and Infection, Faculty of Infectious and Tropical Diseases, London School of Hygiene and Tropical Medicine, London, United Kingdom
2. Department of Pathogen Molecular Biology, Faculty of Infectious and Tropical Diseases, London School of Hygiene and Tropical Medicine, London, United Kingdom
3. Pharmidex Pharmaceutical Services Ltd, 3rd floor, 14 Hanover Street, London, United Kingdom
4. Department of Pharmaceutics, UCL School of Pharmacy, London, United Kingdom

Corresponding author simon.croft@lshtm.ac.uk

ABSTRACT

Disfiguring skin lesions caused by several species of the *Leishmania* parasite characterize cutaneous leishmaniasis (CL). Successful treatment of CL with intravenous (IV) liposomal amphotericin B (LAmB) relies on the presence of adequate antibiotic concentrations at the dermal site of infection within the inflamed skin. Here, we have investigated the impact of the local skin inflammation on the pharmacokinetics (PK) and efficacy of LAmB in two murine models of localized CL (*Leishmania major* and *Leishmania mexicana*) at three different stages of disease (papule, initial nodule and established nodule). Twenty-four hours after administration of 1 x 25 mg/kg LAmB (IV) to infected BALB/c mice (n=5), drug accumulation in skin was found to be dependent on the causative parasite species (*L. major* > *L. mexicana*) and the disease stage (papule > initial nodule > established nodule > healthy skin). Elevated tissue drug levels were associated with increased vascular permeability (Evans Blue assay) and macrophage infiltration (histomorphometry) in the infected skin, two pathophysiological parameters linked to tissue inflammation. After identical treatment of CL in the two models with 5 x 25 mg/kg LAmB (IV), intralesional drug concentrations and reductions in lesion size and parasite load (qPCR) were all ≥ 2-fold higher for *L. major* compared to *L. mexicana*. In conclusion, drug penetration of LAmB into CL skin lesions could depend on the disease stage and the causative *Leishmania* species due to the influence of local tissue inflammation.

KEYWORDS

Cutaneous leishmaniasis, inflammation, pharmacokinetics, liposomal amphotericin B

INTRODUCTION

Leishmaniasis is a vector-borne neglected tropical disease caused by over 20 distinct species of the protozoan *Leishmania* parasite. The two main forms, visceral (VL) and cutaneous leishmaniasis (CL), continue to pose a major public health problem with significant socioeconomic burden worldwide (1). Current estimates show a global annual incidence of one million, 12 million prevalent cases in 98 countries and over 350 million people at risk of infection (2). CL presents as a wide clinical spectrum of skin syndromes, ranging from severe and rare mucosal (MCL), diffuse (DCL) or chronic to the more

common, uncomplicated localized (LCL) lesions. In LCL, single or a limited number of lesions form at the bite site of the parasite-infected female sand fly. A small papule forms, which develops into an initial nodule and then an established nodule with signs of exudation and/or crust formation. The nodule progressively ulcerates and eventually leaves an open wound with raised borders and a crater-like appearance. In most cases, such ulcers slowly self-heal, but leave permanent, disfiguring scars on the exposed skin areas that are often the cause of serious social stigma (3). Tissue damage and disease in CL are primarily caused by an excessive host immune response against the intracellular infection of dermal macrophages by *Leishmania* (4). As the dermis fills with a dense and diffuse mixed inflammatory cell infiltrate (including macrophages, lymphocytes, neutrophils, mast cells and plasma cells), the associated oedema drives swelling of the tissue. Epidermal changes (hyperkeratosis, acanthosis and degeneration of the basal layer), connective tissue damage (collagen lysis) and the formation of non-caseating granuloma can occur (5-9). The immunopathology of LCL shows both similarities (chronic, often ulcerative, dermatosis) and differences (clinical presentation, incubation and resolution time) among different causative *Leishmania* species (10, 11). For example, Old World *L. major* causes so-called 'wet' and acute (early ulcerative) CL lesions in the Middle East: large, irregular and often oozing wounds, which rapidly progress and heal over two to six months (12, 13). In Central America, New World *L. mexicana* is the responsible agent for "chiclero's ulcers", chronic lesions typically found on the ear which spontaneously re-epithelize over a period lasting months to even years (14, 15). In a minority of CL cases caused by *L. major* and *L. mexicana*, alternative types of skin lesions with different clinical presentations and immune response can develop (12-15).

Treatment of CL is problematic; long series of painful injections with the toxic pentavalent antimonials remain the standard therapy (16). A better tolerated, but expensive second-line drug requiring intravenous (IV) administration and cold chain, is AmBisome® (LAmB) (17). LAmB is a unilamellar liposomal formulation of the polyene antibiotic amphotericin B (AmB), which forms cidal pores in the leishmanial cell membranes by ergosterol binding (18). Several treatment regimens for a total cumulative dose of 20-25 mg/kg are efficacious against CL and MCL (19). However, therapeutic responses vary for the different causative *Leishmania* species, populations, geographical regions and clinical settings (20).

We have recently demonstrated that the efficacy of LAmB in murine CL relies on adequate exposure of the active compound amphotericin B (AmB) at the local site of infection, the skin lesion. Moreover, we also showed higher drug disposition in diseased compared to healthy skin (21). Altered pharmacokinetics (PK) at sites of tissue inflammation have been reported previously for antimicrobials (22), anti-inflammatory agents (23) and cancer chemotherapeutics (24). Based on these observations, we formulated three hypotheses.

First, the preferential drug distribution of LAmB in CL lesions over uninfected skin can be explained by the presence and the severity of the local skin inflammation. This could vary among different disease stages of CL and among causative parasite species. In the context of LCL skin inflammation, we have focussed only on aspects potentially relevant to the pharmacological action of liposomal drugs. The inflammatory response against the *Leishmania* infection at the skin inoculation site involves increased vascular permeability and vasodilatation of dermal blood vessels and the infiltration of several types of immune cells including macrophages that play a role in tissue swelling and the formation of skin lesions. Second, the underlying mechanisms for altered drug distribution at the inflammatory site are, at least in part, local capillary leakiness (25-28) and influx of drug-loaded macrophages into the skin (29-34). Third and final, AmB levels accumulating in lesions following LAmB treatment can be source of variability in treatment outcomes against different *Leishmania* species. To test the first two hypotheses, we studied the skin PK of LAmB after administration of a single high dose (1 x 25 mg/kg, IV), as well as pathophysiological parameters that could influence the drug distribution process from blood to skin using the Evans Blue assay (35-37) and histomorphometry. This was done in infected mice and in control mice with variable degrees of skin inflammation: none (uninfected), high (pseudolesion PL, a new mouse model of local skin inflammation based on the rat paw oedema model (38, 39)), or low (healed lesion HL, cure of CL by paromomycin sulphate (40)). Figure 1 gives an overview of the experimental groups and procedures. To investigate the third hypothesis, we compared intralesional drug accumulation and efficacy in *L. major* and *L. mexicana* murine CL following treatment with an identical LAmB dose regimen (5 x 25 mg/kg, IV).

RESULTS

Pharmacokinetic arm: AmB accumulation in skin after LAmB administration.

Figure 2 shows AmB accumulation (ng AmB per gram skin tissue; ng AmB per lesion) in infected and healthy control skin at different stages of murine *L. major* or *L. mexicana* CL (papule, initial nodule, established nodule) 24 hours after administration of a single dose of 25 mg/kg LAmB (IV). The morphology of the lesions is shown in figure 6 (panel a). Table 1 shows AmB lesion-to-healthy-skin-ratios, the ratio of the AmB skin level in the lesion over the AmB skin levels in the healthy control skin (calculated from values in figure 2, row 1). The ratios indicate that there is a 3-fold decrease of intralesional AmB accumulation when LAmB is administered at late (established nodule) compared to early (papule) stages of both *L. major* and *L. mexicana* CL. Drug levels were higher in *L. major* than in *L. mexicana* lesions at all stages of disease. Disposition of AmB in the PL was significantly higher than in healthy skin ($p<0.0001$). In contrast, AmB accumulation in HL is not significantly different to that in healthy control skin ($p=0.37$) and is similar to the baseline levels in uninfected mice. Drug distribution patterns are highly comparable when AmB concentrations are expressed relative (normalized, ng/g) or absolute (ng/lesion). This indicates that the altered PK of LAmB at different stages of CL is not a consequence of bias introduced by change in tissue volume/weight over the course of infection.

Skin pathophysiology arm: factors affecting the PK of LAmB.

Lesion characterisation: size and parasite load. Figure 3 shows the lesion characteristics (top row: lesion size, bottom row: parasite load) at different stages of infection by *L. major* or *L. mexicana* CL (papule, initial nodule, established nodule). The morphology of the lesions can be seen in figure 6 (panel a). *L. major* lesions increased in size at a more rapid pace than *L. mexicana*, with different parasite load dynamics over time. During the 20 days following infection with *L. major*, lesion size gradually increased from 0 to around 7 mm and parasite load remained stable from day 5. Following infection with *L. mexicana*, smaller lesions formed (up to 5 mm) and the parasite load gradually increased. The PL swelling of rump skin had a size comparable to CL lesions, but as expected, no parasites could be detected in this *Leishmania*-free type of skin inflammation. In contrast, the HL (day 20, after 10-day treatment with paromomycin) had a lesion size of 0 ± 0 mm and parasite load was around a 100-fold lower than in the untreated *L. major* established nodules (day 20). As expected, neither lesion size nor parasite load was measurable in uninfected mice.

Evans Blue: leakiness of dermal capillaries. Figure 4 shows vascular permeability in infected and healthy control skin at different stages of murine *L. major* or *L. mexicana* CL (papule, initial nodule, established nodule), as evaluated by the Evans Blue Assay. The morphology of the lesions can be seen in figure 6 (panel a). Table 1 shows Evans Blue lesion-to-healthy-skin-ratios, the ratio of the Evans Blue skin level in the lesion over the Evans Blue skin levels in the healthy control skin (calculated from the values in figure 4). The ratios for *L. major* indicate that, compared to healthy control skin, vascular permeability is 6-fold higher in papules and 9-fold higher in initial nodules and established nodules. For *L. mexicana*, there is 3-10 fold increase in permeability compared to healthy skin and the increase is comparable at papular, nodular and established noduleative stages. Blood vessel leakiness was 12-fold higher ($p<0.0001$) in the PL than in healthy skin. In HL, vascular permeability is not significantly different to that in healthy control skin ($p=0.99$) and is similar to the baseline levels in uninfected mice. In the photos in figure 4, the intense blue coloration of lesions (due to accumulation of the dye Evans Blue) provides an additional, qualitative confirmation of capillary leakiness at the site of infection. Such a phenomenon in absent in healthy skin tissues.

Skin histomorphometry: inflammatory cells and macrophages. Figure 5 shows the number of total cells (top row) and the abundance of macrophages (bottom row) in infected and healthy control skin at different stages of murine *L. major* or *L. mexicana* CL (papule, initial nodule, established nodule). Figure 6 shows the morphology of the lesions (panel a), the H&E stain (panel b) and the anti-Iba-1 stain (panel c). Figure 7 examines the H&E and Iba-1 stains of CL lesions in more detail. Table 1 shows total cell and macrophage lesion-to-healthy-skin-ratios, the ratio of the total cell and macrophage skin numbers in the lesion over the total cell and macrophage skin numbers in the healthy control skin (calculated from the values in figure 5). The ratios indicate that the number of cells in the tissue doubles in CL lesions as the disease progresses and a large fraction of the infiltrated inflammatory cells are macrophages. However, the number of inflammatory cells and macrophages in *L. major* lesions are higher than those in *L. mexicana* lesions at all stages of disease. In the PL, the number of inflammatory cells were significantly higher than in healthy skin ($p=0.0034$), but this was not the case for macrophages specifically ($p>0.99$). In the HL, the number of inflammatory cells and macrophages were not significantly different to that in healthy control skin ($p>0.05$) and are similar to the baseline levels in uninfected mice.

Relation between PK and pathophysiology parameters. Table 1 shows the lesion-over-healthy-skin-ratios (parameter value in lesion / parameter value in healthy skin) for AmB accumulation (figure 2 data, AmB levels in ng/g), blood vessel permeability (figure 4 data), number of cells and number of macrophages (figure 5 data). For uninfected mice, the ratios for AmB, blood vessel permeability, cell numbers and macrophage numbers were around 1, indicating no difference in the values for these parameters between the lesion site (rump skin) and the healthy site (back skin). Comparing *Leishmania*-infected mice to uninfected mice, AmB accumulation, blood vessel permeability, cell numbers and macrophage numbers were higher at all three stages of disease for both *L. major* and *L. mexicana*. However, these ratios were increased for *L. major* compared to *L. mexicana*. The higher ratios for PL compared to uninfected mice indicate increased drug accumulation as well as blood vessel leakiness, cell numbers and macrophages in this alterative type of skin inflammation. For HL, however, all lesion-over-healthy ratios were highly similar to the baseline ratios found in healthy mice (except for macrophage number). Similar patterns at different stages of disease were found in *L. major* and *L. mexicana*-infected mice. A significant increase in ratios for drug accumulation, blood vessel permeability, cell numbers and macrophage numbers was found in papules (early CL) compared to uninfected mice. Comparing ratios for the papule compared to those for initial nodules and established nodules (later-stage CL), relatively little new, additional inflammatory cells and macrophages seemed to infiltrate the skin (for both *L. major* and *L. mexicana*) and blood vessel permeability remained stable (for *L. major* but not *L. mexicana*).

Skin PK and efficacy of LAmB in CL.

Finally, we evaluated the efficacy of LAmB against *L. major* and *L. mexicana* in the BALB/c mouse model of CL. Figure 8 shows *in vivo* activity and intralesional AmB accumulation on day 10, after treatment of mice with initial nodules with 5 doses of 25 mg/kg LAmB (IV) on alternate days (i.e. on day 0, 2, 4, 6 and 8). LAmB showed *in vivo* activity against both CL-causing parasite species. However, reductions in lesion size and parasite load compared to untreated controls were greater and significant for *L. major* (p=0.011 and 0.0471) compared to *L. mexicana* (p=0.25 and 0.99). We also observed almost 2-fold higher AmB levels (ng/g) in *L. major* over *L. mexicana* lesions. In CL-infected skin, drug levels concentrations were at least 4-fold higher comparing to healthy rump skin of identically uninfected LAmB treated mice. However, this difference was significant for *L. major*

(p<0.0001) but not for *L. mexicana* (p=0.15). The *L. major* data has already been reported earlier (21), but is included to enable direct comparison with *L. mexicana* (novel data).

DISCUSSION

Local tissue inflammation in infectious disease can alter the pharmacokinetics (PK) and thus therapeutic outcomes of antimicrobials (41-43). In this work, we have confirmed our hypothesis that the inflamed state of skin lesions in CL alters the PK of liposomal amphotericin B (LAmB) following intravenous drug administration in two mouse models of infection. Our results show that AmB accumulation in CL-infected skin is (i) *Leishmania* species-specific (*L. major* > *L. mexicana* lesions) (ii) disease-stage-specific (papule > initial nodule > established nodule > healthy skin) and (iii) a plausible cause of the superior *in vivo* efficacy of LAmB against *L. major* compared to *L. mexicana*.

Firstly, the preferential distribution of LAmB to CL infection sites (*L. major* > *L. mexicana*) compared to uninfected ones could be explained by the presence and the severity of the local inflammatory response against the parasites residing in dermal macrophages. Compared to *L. mexicana*, *L. major* causes more heavily inflamed (exudative) established nodules with a more rapid, aggressive onset in humans (12-15) and mice (3, 44). Several quantitative biomarkers for skin inflammation in our study confirmed this. Leakiness of the dermal capillaries, swelling/oedema in the skin tissue (indicated by lesion size) and numbers of infiltrating macrophages or other inflammatory cells were higher in *L. major* compared to *L. mexicana* CL, at all stages of disease. These findings are consistent with earlier reports (45-47). Moreover, the HL and PL observations support this inflammation-driven theory of enhanced drug accumulation. When the inflammation in *L. major*-infected skin is largely cleared because of parasite elimination by paromomycin treatment (HL), AmB accumulation, blood vessel permeability and cell numbers return to baseline levels seen in uninfected skin. However, when inflammation is experimentally induced by injection of λ- carrageenan (instead of parasites) in rump skin (similar site as in CL-infection), the local drug concentrations after LAmB administration also increase by over 3-fold. Such a phenomenon could be explained by a 10-fold increase in leakiness of the skin capillaries. The new PL model of local skin inflammation, based on subcutaneous injection of λ-carrageenan, could be a useful research tool for dermatoses other than CL, such as skin cancers, atopic dermatitis or psoriasis (48).

Secondly, the increased intralesional AmB accumulation after intravenous LAmB dosing of mice with CL in earlier stages of disease (papule > initial nodule > established nodule) could be related to changes in infiltration of phagocytes prone to internalize circulating liposomes and, likely to lesser degree, capillary leakiness in the dermis. When LAmB is administered to mice with early CL, during the initial massive influx of phagocytes and inflammatory cells into the skin as part of the antileishmanial immune response (4, 11), intralesional drug levels could be increased as AmB-loaded cells migrate from the blood stream to the infection site. Hence, in later stages of disease, when the number of additional macrophages infiltrating the infected tissue is more limited, skin AmB accumulation could be lower. The known role of phagocyte transport in the delivery of various antibiotics (30-32), including liposomal AmB (41), to local infection sites, as well as our PK and histology data suggests the plausibility of this hypothesis. Confirmative research should distinguish extra- and intracellular levels in circulating and dermal macrophages after LAmB administration. While phagocytes can increase AmB exposure in the lesion, their therapeutic relevance is still unclear. Cellular lysis, resulting in local release of the drug payload, or impaired parasite survival in these 'pretreated' macrophages could play a role. Another pathophysiological factor affecting the PK of LAmB is blood vessel leakiness, a result of vasodilatation and enhanced vascular permeability in the inflamed dermis. Here, we confirmed the existence of this phenomenon in experimental CL for the first time. It could facilitate extravasation of the liposomes (~ 80 nm in size) through the dermal capillaries, which under normal physiological conditions have a pore cut-off size of 6-12 nm (21). However, it cannot explain a decrease in AmB disposition in lesions as CL progresses by itself, because we found comparable degrees of capillary leakage similar in papules, initial nodules and established nodules. Other factors that could affect cellular and dermal PK, such as plasma and tissue protein-binding (49), angiogenesis (50), lymphatic drainage, phagocytic capacity and activation stage of (parasitized) macrophages (33), skin metabolism, clearance by the reticuloendothelial system (51), or the involvement of (non-macrophage) immune cells, mediators or responses, were not evaluated in this study. A similar trend of decreasing drug distribution of LAmB to target organs during later disease stages was also found in murine VL (33). However, interestingly, *Leishmania*-infected livers contain lower rather than higher drug levels compared to healthy ones.

Thirdly, the *in vivo* activity of LAmB was superior against *L. major* compared to *L. mexicana*, likely due to inflammation-enhanced and relatively increased drug levels at the infection site. A clear correlation

between drug levels of the leishmanicidal, concentration-dependent antibiotic AmB delivered to the lesion and the efficacy of LAmB in murine CL has already been reported (21, 52). Apart from skin PK, there could be also be differences in antileishmanial pharmacodynamics (PD) and the resulting PK/PD relationship. An intrinsic species-specific sensitivity to the active compound AmB is unlikely, as *in vitro* EC_{50} values are comparable (≈ 0.1 µM) (35). However, the *in vivo* susceptibility could still vary based on the metabolic state of the *L. major* or *L. mexicana* parasites in the skin. In chronic lesions with slow disease onset, a quiescent, semi-dormant phenotype of *L. mexicana* could exist, benefitting its long-term survival and possibly showing reduced drug sensitivity (53-55). Such PK/PD factors could cause variable rate or magnitude of parasite elimination, a combined outcome of drug activity and host immunity. Pharmacogenetic differences between individual patients and populations (affecting distribution, metabolism and clearance) might also contribute to additional variation in LAmB efficacy in the clinic (20).

Finally, although BALB/c mice are common in PK studies (56) and *L. major*-BALB/c is a highly reproducible and well-established model for antileishmanial drug evaluation (57), differences between CL in humans (mostly self-curing lesions) and BALB/c mice (non-healing lesions) (58) should be considered. Our studies used mice with relatively small (< 1 cm), local and uncomplicated CL lesions. Despite variation in the immunological nature of the skin inflammation, the phenomena of capillary leakiness, oedema formation and phagocyte infiltration occur in both mice and humans (59, 60). Thus, our findings could hold treatment implications for CL as well as for other inflammatory (skin) disorders. During preclinical evaluation of novel nanoparticles, a drug delivery strategy used for CL (61), the time of drug administration (relative to disease stage) and causative species are important factors that can affect both PK and PD. In the clinic, LAmB treatment outcomes in CL are already known to relate to the causative *Leishmania* species. A recent observational study in a group of travellers with (M)CL (20) reported differences in the therapeutic success rate of LAmB against *L. infantum* (78%), *L. major* (50%) and *Leishmania Viannia* subgenus species (28%). However, because *L. mexicana* was not included in this work, we can not directly compare our results in mice to those in humans. In addition, early diagnosis and therapeutic intervention with LAmB could produce enhanced drug exposure in the skin lesion. No present clinical studies have reported on this. In contrast, early treatment of *L. brasiliensis* CL with intramuscular pentavalent antimonials was associated with a 5-fold increased risk of treatment failure (62, 63). Both the impact of parasite species and the age of the

287 lesion in CL on PK and therapeutic efficacy of LAmB (and other antileishmanial drugs) deserve further
288 investigation. Laboratory experiments could investigate outcomes of multi-dose treatments in
289 alternative models of disease caused by additional *Leishmania* species and strains. Extrapolation of
290 LCL results to the various types of complex CL is complicated by differences in histopathology (blood
291 vessel destruction in advanced MCL (10)) and the nature and severity of the inflammatory response
292 (balance TH1/TH2-type cellular immunity in local *versus* diffuse CL (3, 4)). Overall, it is clear that the
293 immunohistopathology of CL has a profound impact on drug disposition of antileishmanial agents,
294 both when administered topically (increased permeation through the damaged epidermis (64, 65))
295 and systemically (enhanced extravasation for liposomal and non-encapsulated drugs (21)).

296 In conclusion, our data indicates that the severity of inflammatory skin disease in CL could contribute
297 to variable drug penetration in the target tissue and therapeutic efficacy of LAmB. The significant
298 impact of local inflammation on PK and PK/PD is not only an important consideration for the
299 development of new drugs and clinical dose regimens for the treatment of CL, but also for other
300 (infectious) diseases with an inflammatory component.

301

302 **MATERIALS AND METHODS**

303 **Parasites, media and drugs.** *L. major* MHOM/SA85/JISH118 and *L. mexicana* MNYC/BZ/62/M379
304 parasites were cultured in Schneider's insect medium (Sigma, UK) supplemented with 10% heat-
305 inactivated fetal calf serum (HiFCS, Sigma UK). These were passaged each week at a 1:10 ratio of
306 existing culture to fresh media in 25 ml culture flasks without filter and incubated at 26 °C. For
307 infection of mice, stationary phase parasites were centrifuged for 10 minutes at 2100 rpm and 4 °C.
308 The supernatant was removed and the pellet re-suspended in RPMI medium (Sigma, UK). Cell
309 number was estimated by microscopic counting with a Neubauer haemocytometer. AmBisome®
310 (LAmB, Gilead, UK) was reconstituted with 12 ml sterile water (as per the manufacturer's instructions)
311 to yield a stock solution of 4 mg/ml and diluted in 5% aqueous dextrose to achieve a drug dose of 25
312 mg/kg. Paromomycin sulphate (Sigma, UK) was prepared in phosphate buffered saline (PBS) to yield
313 50 mg/kg doses. λ-carrageenan (Sigma, UK) and Evans Blue (Sigma UK) 0.5 % (w/v) solutions were
314 made up in phosphate buffered saline (PBS, Sigma, UK). Drug preparations were stored at 4 °C
315 during the experiments.

Experimental groups. Female BALB/c mice around 6-8 weeks old and a mean weight of 18-20 g were purchased from Charles River Ltd (Margate, UK). These were kept in humidity and temperature controlled rooms (55-65%, 25-26 °C) and fed water and rodent food *ad libitum*. Mice were randomized and allowed an acclimatization time of one week. All animal experiments were conducted under license 70/8427 according to UK Home Office regulations under the Animals (Scientific Procedures) Act 1986 and EC Directive 2010/63/E. An overview of the groups is shown in figure 1.

1. *L. major* CL. Mice were subcutaneously (SC) infected in the shaven rump above the tail with 200 µl parasite suspension containing 4 x 10^7 of low passage number (P<5), stationary phase *L. major* promastigotes in RPMI medium. Lesion size was measured daily with digital callipers (average of length and width) after inoculation as the CL lesions developed into papules, initial nodules and established nodules. In this animal model of CL, these respective disease stages occurred on day 5, 10 and 20, as shown previously (40). We define a 'CL lesion' as a stationary, local skin abnormality at the site of *Leishmania* parasite inoculation (rump). A 'papule' is the smallest (2-4 mm) CL lesion, a palpable elevation of the skin with no signs of ulceration. An 'initial nodule' is a medium-sized (4-6 mm) papule that is larger and more defined. An 'established nodule' is a larger (5-8 mm) CL lesion that is crusted or exudative.
2. *L. mexicana CL*. Mice were infected as described above for *L. major*, but *L. mexicana* promastigotes were used. In this animal model of CL, the disease stages of papule, initial nodule and established nodule occurred on days 15, 30 and 45 post-inoculation (40). The earlier definitions of 'CL lesion', 'papule', 'initial nodule' and 'established nodule' apply.
3. Skin inflammation controls. For the uninfected controls, mice were infected in the shaven rump above the tail with 200 µl parasite-free RPMI medium (SC). For the 'healed lesion' (HL) controls, mice with *L. major* initial nodules (10 days post-inoculation, infection as described above) were treated daily for 10 days with 50 mg/kg paromomycin sulphate in PBS (200 µl via the intraperitoneal (IP) route). This regimen has proven efficacy in the *L. major*-BALB/c model of CL (40). A size of 0 mm (complete disappearance of the skin lesion) was considered a near-complete healing and a negative control for skin inflammation. For the 'pseudolesion' (PL) control, mice were SC injected in the shaven rump above the tail with 25 µl 0.5 % λ-carrageenan in PBS. After 24 hours, when a measurable lesion-like but parasite-free swelling

of skin had occurred, the pseudolesion was considered a positive control for skin inflammation. These specific concentration and time points were chosen based on similarity to CL-lesions and experimental requirements. The resulting diameter of the skin swelling ("lesion size") was between 2-8 mm (the size of our CL lesions). Moreover, the local inflammation remained for at least 48 hours (24 hours to reach maximal swelling and another 24 hours for PK experiment). This novel carrageenan-induced model of local rump skin inflammation in mice was based on the well-established model of rat paw inflammation (38, 39) and preparatory studies are shown in Supplement 1.

Procedures per experimental group. Ten mice per group (*L. major* papule, *L. major* initial nodule and *L. major* established nodule; *L. mexicana* papule, *L. mexicana* initial nodule and *L. mexicana* established nodule; uninfected, pseudolesion and healed lesion) were divided in a pharmacokinetic (n=5) and skin pathophysiology arm (n=5). This allowed simultaneous studying of drug accumulation 24 hours after LAmB administration (this time point results in maximal AmB accumulation in skin(21)) and pathophysiology factors affecting pharmacokinetics at the time of drug administration (30 minutes after administration of Evans Blue, standard time for preferential distribution of the dye to inflamed compared to healthy peripheral tissue sites (35-37)). An overview of the procedures performed per group is shown in figure 1.

- **Pharmacokinetic arm**. Each animal in this arm (n=5) received an IV bolus (200 µl) of LAmB at a dose level of 25 mg/kg. Twenty-four hours later, animals were sacrificed and skin samples (from lesion and healthy control site) were collected. The skin samples were homogenised and AmB levels in tissues measured as previously described (21, 33). Briefly, skin tissues were ground mechanically with zirconium oxide beads in 1 ml of PBS. The drug (AmB) was then extracted from tissue homogenates with 84:16 methanol:DMSO, followed by LC-MS/MS quantification. When the expression 'AmB levels' or 'AmB concentrations' is used in this work without further clarification, it refers to total (liposomal + protein-bound + 'free') amount of AmB per gram of tissue. Pharmidex Pharmaceutical Services Ltd. performed LC-MS/MS analysis of the samples. The lower limit of quantification was 1 ng/ml.
- **Skin pathophysiology arm**. Each animal in this arm (n=5) received an intravenous bolus (200 µl) of 0.5 % Evans Blue (Sigma, UK). Lesion size (average of width and length, mm) was measured with digital callipers. Thirty minutes later, animals were sacrificed and skin samples

(from the lesion and the healthy control site) were collected. These samples were cut into three equal parts, weighed and used for the following evaluations:

1. Capillary leakiness. The first skin fragment was used to evaluate blood vessel leakiness with the Evans Blue assay. Evans Blue is a blue dye, which is, under normal physiological conditions, predominantly restricted to the blood stream because of high plasma protein binding. However, the protein-dye complex can extravasate at sites of increased vessel leakiness, as is the case in local inflammation. Hence, the amount of Evans Blue per gram of tissue is a marker for local vascular permeability (35-37). To extract Evans Blue from skin, tissue sections were placed in 500 µl formamide in Eppendorf tubes and incubated in a 55 °C water bath. After 24 hours, tubes were centrifuged for 10 minutes at 15000 rpm at 4 °C and supernatants were collected. Absorbance (maximum 620 nm, minimum 740 nm) was determined with a Spectramax M3 plate reader (Molecular Devices, UK). Samples, blanks (formamide) and calibration standards (1:2 serial dilution of 100 µg/ml Evans Blue in formamide) were measured in 96-well plates (200 µl volumes). After correction against the blank, the amount of Evans Blue in samples was expressed per gram of skin tissue.
2. Parasite load. The second skin tissue fragment was used to evaluate *L. major* and *L. mexicana* parasite loads with DNA-based quantitative PCR, as described previously (40). In brief, skin tissue was homogenised and DNA extracted with a Qiagen DNAeasy® kit for blood and tissue. Two µl DNA extract samples (1/100 diluted) were amplified in 10 µl reactions in the presence of 5 µl SensiFAST SYBR® NO-ROX master mix, 0.25 µM probe and 0.4 µM primers. Triplicates of standards (10^8 to 10^2) and duplicates of unknown samples were included. The tubes were placed in a 72 sample rotor of the RotorGene 3000, set at 40 cycles at a denaturation setting of 95 °C for 5 minutes followed by a 2-step amplification cycle of 95 °C for 10 seconds and 60 °C for 30 seconds. The lower limit of quantification was 100 parasites per 2µl.
3. Skin histomorphometry. The third and final skin fragment was fixed in formalin for 24 hours, dehydrated in ethanol, cleared in xylene and embedded in paraffin. Skin samples were stained with haematoxylin and eosin (H&E) or antibodies against the macrophage/microglia-specific protein iba-1 (anti-Iba 1). All histological procedures were

performed at the Institute of Neurology (UCL, London, UK) and blind analysis using the same analyst was conducted at LSHTM. Leica ST5020 Autostainer was used for H&E stain, according to the standard NHS diagnostic protocol. Randomly selected images covering skin regions were acquired with a camera (Leica DFC295) attached to a Leica DM3000 LED microscope. Images were digitalized for histomorphometric analysis using the Leica Application Suite V4.5 software. An index of inflammatory cells was assessed by quantifying a standardized test area of 166970.7 μm^2 per image acquired, with 20x objective. The number of cells/image was determined from the average of 6 images/animal, randomly chosen, at 200x magnification, stained with H&E. An increase in the number of cells compared with uninfected controls was considered indicative of inflammation. Immunohistochemistry reaction for macrophage presence was performed using the Ventana Discovery XT using the Ventana DAB Map detection Kit. Tissues were pre-treated for 40 minutes with EDTA buffer, incubated for 4 hours with the primary antibody (anti-Iba-1, 1/250 dilution, Wako Laboratory Chemicals, Germany) and treated with Swine anti Rabbit Dako E0353 for 1 hour (manufacturers protocol). The polyclonal antibodies in the anti-Iba-1 stain label the calcium-binding protein iba-1, specific to microglia (central nervous system) and macrophages (skin and other tissues). An index of macrophage was assessed by quantifying a standardized test area of 166970.7 μm^2 per image, acquired with 20 x objective. The area in brown was determined from an average of 6 randomly chosen images/animal, at 200x magnification. Increased stained area compared with uninfected controls was considered indicative of macrophage infiltration.

Efficacy of LAmB against *L. major* and *L. mexicana*. Uninfected or *Leishmania*-infected BALB/c mice with nodular CL lesions (10 and 30 days post-inoculation for *L. major* and *L. mexicana*, respectively) received five doses (200 µl, IV) of either 5% dextrose (untreated control) or LAmB at 25 mg/kg (treated) on alternate days (i.e. on day 0, 2, 4, 6, 8). During treatment, lesion size was monitored daily. On day 10, animals were sacrificed, lesion samples were collected and parasite load and AmB drug levels in these tissues quantified (see above).

Statistical analysis. For the PK and pathophysiology experiments, intralesional AmB accumulation, lesion size, parasite load, capillary leakiness, cell number and macrophage abundance were compared in infected and uninfected skin of the same mice using a 2-way ANOVA followed by Sidak

multiple comparison test. For the efficacy experiment, ANOVA (1-way for parasite load and intralesional AmB levels, 2-way repeated measures for lesion size) followed by Tukey's multiple comparison test was used. Data is presented as mean and standard error of the mean (SEM). A p-value < 0.05 was considered statistically significant. All analyses were performed with GraphPad Prism version 7.02.

TABLES

Table 1: Lesion-over-healthy-skin-ratios, based on the values found in lesions (rump) and healthy control skin (back) for the following of the variables: AmB accumulation, blood vessel permeability, total number of cells, and number of macrophages. Data derived from figures 2, 4 and 5.

	L. major CL			*L. mexicana* CL			Controls		
	papule	initial nodule	established nodule	papule	initial nodule	established nodule	Uninf	PL (+)	HL (-)
AmB accumulation	16.2	2.5	1.2	3.7	2	1.6	0.5	3.2	0.5
Blood vessel permeability	5.9	9.4	6.8	2.6	12.5	9.5	1.7	11.7	1.2
Number of cells	1.8	2.3	2.4	1.2	1.2	1.4	1	1.6	1.1
Number of macrophages	5.4	7.2	5.1	3	4.8	4.9	0.9	1.5	4.8

FIGURES

Figure 1: Schematic overview of experimental design to study the influence of skin inflammation in CL on the PK of LAmB.

451 **Figure 2**: Skin accumulation of amphotericin B (AmB), 24 hours after a single intravenous (IV)
452 administration of 25 mg/kg AmBisome (LAmB) to CL-infected mice at different time points post-
453 infection and controls. Drug levels were determined in the lesion (●) and healthy control skin (○) site
454 for each animal. CL-infected mice with skin lesions were dosed with LAmB at the time when a papule,
455 an initial nodule or an established nodule was present on the rump (respectively: 5, 10 and 20 days
456 after *L. major* infection; 15, 30 and 45 days after *L. mexicana* infection). Controls for skin
457 inflammation: uninfected mice (uninf), pseudolesion PL (mice with carrageenan-induced inflammatory
458 skin initial nodule) and healed lesion HL (mice with paromomycin-cured *L. major* initial nodule). Data:
459 means ± SEM (n=3-5 per group). Statistical analysis: 2-way ANOVA followed by Sidak multiple
460 comparison test. *= p<0.05, **= p <0.01, ***= p<0.001, ****= p<0.0001.

461 **Figure 3**: Lesion size (top row) and parasite load (bottom row) in to CL-infected mice at different time
462 points post-infection and controls. Lesion size (mm) and parasite load (parasites per gram skin) were
463 determined in the lesion (●) and healthy control skin (○) for each animal. CL-infected mice with skin
464 lesions were measured at the time when a papule, an initial nodule or an established nodule was
465 present on the rump (respectively: 5, 10 and 20 days after *L. major* infection; 15, 30 and 45 days after
466 *L. mexicana* infection). Controls for skin inflammation: uninfected mice (uninf), pseudolesion PL (mice
467 with carrageenan-induced inflammatory skin initial nodule) and healed lesion HL (mice with
468 paromomycin-cured *L. major* initial nodule). Data: means ± SEM (n=3-5 per group). Statistical
469 analysis: 2-way ANOVA followed by Sidak multiple comparison test. *= p<0.05, **= p <0.01, ***=
470 p<0.001, ****= p<0.0001.

471 **Figure 4**: Leakiness of the bloods vessels in the skin of CL-infected mice at different time points post-
472 infection and controls. After administration of Evans Blue (200 µl 0.5%, IV), the amount of the blue
473 dye per gram of tissue was determined in the lesion (●) and healthy control skin (○) for all animals.
474 CL-infected mice with skin lesions were dosed with Evans Blue at the time when a papule, an initial
475 nodule or an established nodule was present on the rump (respectively: 5, 10 and 20 days after *L.*
476 *major* infection; 15, 30 and 45 days after *L. mexicana* infection). Controls for skin inflammation:
477 uninfected mice (uninf), pseudolesion PL (mice with carrageenan-induced inflammatory skin initial
478 nodule) and healed lesion HL (mice with paromomycin-cured *L. major* initial nodule). Data: means ±
479 SEM (n=3-5 per group). Statistical analysis: 2-way ANOVA followed by Sidak multiple comparison

test. *= p<0.05, **= p <0.01, ***= p<0.001, ****= p<0.0001. The picture shows *L. major*-infected mice (day 10) after 30 minutes after administration of Evans Blue (IV). The arrows point at the blue coloration of the CL lesions (before skin sample collection, left photo) as well as intense blue staining of the underlying thoracolumbar fascia (after skin sample collection, right photo).

Figure 5: Estimation of the number of cells (top row, H&E stain) and macrophages (bottom row, anti Iba-1-reaction) at the infected lesion site (rump skin, black bars) and the control site (back skin, white bars) of control mice and CL-infected mice. Measurements in CL-infected mice with skin lesions were performed at the time when a papule, an initial nodule or an established nodule was present on the rump (respectively: 5, 10 and 20 days after *L. major* infection; 15, 30 and 45 days after *L. mexicana* infection). Controls for skin inflammation: uninfected mice (uninf), pseudolesion PL (mice with carrageenan-induced inflammatory skin initial nodule) and healed lesion HL (mice with paromomycin-cured *L. major* initial nodule). Standard surface: picture area showing full skin tissue (epidermis, dermis and hypodermis) to allow direct comparisons among groups (166970.7 μm^2). Data: means ± SEM (n=3-5 per group). Statistical analysis: 2-way ANOVA followed by Sidak multiple comparison test. *= p<0.05, **= p <0.01, ***= p<0.001, ****= p<0.0001.

Figure 6: Collage panels of murine skin lesions developed during CL disease progress and controls for skin inflammation. Per panel: photo of the lesion on the rump of the mice (a, white arrow points at lesion), haematoxylin and eosin stain (b, purple arrow points at a cluster of inflammatory cells) and macrophage marker anti-ionized calcium binding adapter molecule 1-antibody stain (c, brown arrow points at a cluster of macrophages). Top row: controls for skin inflammation (uninfected, pseudolesion and healed lesion). Middle row: *L. major* CL lesions (papule present 5 days post-infection, initial nodule present 10 days post-infection and an established nodule present 20 days post-infection). Bottom row: *L. mexicana* CL lesions (papule present 15 days post-infection, initial nodule present 30 days post-infection and an established nodule present 45 days post-infection). Black bar in (b) = 100 µm.

Figure 7: Comparison of mouse skin morphology and macrophage density in healthy, uninfected skin (left), *L. major* CL lesion (20 days post-infection, middle) and *L. mexicana* CL lesion (45 days post-infection, right). The central picture in each panel (H&E stain) shows the structural layers of the skin: epidermis (E), dermis (D) and hypodermis (H), with the underlying muscle (M) at x 4 magnification

(bar = 100 µm). The inserts (1-4) highlight details of the central picture (x 80 magnification, bar =10 µm). ①: epidermis. ②: dermal capillaries. ③: *Leishmania* amastigotes within parasitophorous vacuoles. ④: anti-iba-1 stain (macrophage marker) of tissue shown in insert ③. In both the *L. major* and *L. mexicana* CL lesion, intense inflammatory foci (I) are present in the skin, causing severe disruption the D and H architecture. Compared to healthy, uninfected skin, CL lesions also showed (i) epidermal hyperplasia and acanthosis for *L. mexicana* but not for *L. major* (①), (ii) dilated blood vessels, a factor contributing to capillary leakiness (②) and (iii) a large amount of inflammatory cells (③), many of which are macrophages (④).

Figure 8: Efficacy and biodistribution of liposomal amphotericin B LAmB) in murine models *L. major* and *L. mexicana* CL. Mice were injected (SC) with parasite-free medium (uninfected) or infected with *L. major* or *L. mexicana* promastigotes in the rump skin. When a nodular lesion had formed at the inoculation site of CL-infected animals (10 and 30 days post-inoculation for *L. major* and *L. mexicana*, respectively), animals received either 5% dextrose (untreated) or 25 mg/kg LAmB (IV) on days 0, 2, 4, 6 and 8. During treatment, lesion size (a) was measured daily. On day 10, lesion skin tissues were collected and parasite load (b) and AmB levels (c) determined. Each point represents mean ± SEM (n=3-5 per group). ANOVA (1-way for parasite load and intralesional AmB levels, repeated measures for lesion size), followed by Tukey's multiple comparison test (* = p<0.05, **** =p<0.0001, ns = not significant). N/A: not applicable.

ACKNOWLEDGEMENTS

Gert-Jan Wijnant's doctoral project is part of the EuroLeish.Net Training Network (www.euroleish.net). This work was supported by the European Horizon's 2020 Research and Innovation Programme under the Marie Sklodowska-Curie grant agreement number 642609.

REFERENCES

1. Okwor I, Uzonna J. 2016. Social and Economic Burden of Human Leishmaniasis. Am J Trop Med Hyg 94:489–493.

2. Alvar J, Vélez ID, Bern C, Herrero M, Desjeux P, Cano J, Jannin J, den Boer M. 2012. Leishmaniasis Worldwide and Global Estimates of Its Incidence. PLoS One 7.
3. Scorza BM, Carvalho EM, Wilson ME. 2017. Cutaneous Manifestations of Human and Murine Leishmaniasis. Int J Mol Sci 18.
4. Scott P, Novais FO. 2016. Cutaneous leishmaniasis: immune responses in protection and pathogenesis. Nat Rev Immunol 16:581–592.
5. Cangussú SD, Souza CC de, Campos CF, Vieira LQ, Afonso LCC, Arantes RME. 2009. Histopathology of Leishmania major infection: revisiting L. major histopathology in the ear dermis infection model. Mem Inst Oswaldo Cruz 104:918–922.
6. Corware K, Harris D, Teo I, Rogers M, Naresh K, Müller I, Shaunak S. 2011. Accelerated healing of cutaneous leishmaniasis in non-healing BALB/c mice using water soluble amphotericin B-polymethacrylic acid. Biomaterials 32:8029–8039.
7. Gaafar A, el Kadaro AY, Theander TG, Permin H, Ismail A, Kharazmi A, el Hassan AM. 1995. The pathology of cutaneous leishmaniasis due to Leishmania major in Sudan. Am J Trop Med Hyg 52:438–442.
8. Andrade ZA, Reed SG, Roters SB, Sadigursky M. 1984. Immunopathology of experimental cutaneous leishmaniasis. Am J Pathol 114:137–148.
9. Kaye PM, Beattie L. 2016. Lessons from other diseases: granulomatous inflammation in leishmaniasis. Semin Immunopathol 38:249–260.
10. Nylén S, Eidsmo L. 2012. Tissue damage and immunity in cutaneous leishmaniasis. Parasite Immunol 34:551–561.
11. Mehregan DR, Mehregan AH, Mehregan DA. 1999. Histologic diagnosis of cutaneous leishmaniasis. Clin Dermatol 17:297–304.
12. Bari AU. 2012. Clinical spectrum of cutaneous leishmaniasis: an overview from Pakistan. Dermatol Online J 18:4.
13. Abuzaid AA, Abdoon AM, Aldahan MA, Alzahrani AG, Alhakeem RF, Asiri AM, Alzahrani MH, Memish ZA. 2017. Cutaneous Leishmaniasis in Saudi Arabia: A Comprehensive Overview. Vector Borne Zoonotic Dis 17:673–684.
14. Blaylock JM, Wortmann GW. 2012. A case report and literature review of “Chiclero’s Ulcer”. Travel Med Infect Dis 10:275–278.

15. Calvopiña M, Martinez L, Hashiguchi Y. 2013. Cutaneous leishmaniasis “chiclero’s ulcer” in subtropical Ecuador. Am J Trop Med Hyg 89:195–196.
16. Hodiamont CJ, Kager PA, Bart A, de Vries HJC, van Thiel PPAM, Leenstra T, de Vries PJ, van Vugt M, Grobusch MP, van Gool T. 2014. Species-Directed Therapy for Leishmaniasis in Returning Travellers: A Comprehensive Guide. PLoS Negl Trop Dis 8.
17. Balasegaram M, Ritmeijer K, Lima MA, Burza S, Ortiz Genovese G, Milani B, Gaspani S, Potet J, Chappuis F. 2012. Liposomal amphotericin B as a treatment for human leishmaniasis. Expert Opin Emerg Drugs 17:493–510.
18. Wortmann G, Zapor M, Ressner R, Fraser S, Hartzell J, Pierson J, Weintrob A, Magill A. 2010. Lipsosomal Amphotericin B for Treatment of Cutaneous Leishmaniasis. Am J Trop Med Hyg 83:1028–1033.
19. Aronson N, Herwaldt BL, Libman M, Pearson R, Lopez-Velez R, Weina P, Carvalho E, Ephros M, Jeronimo S, Magill A. 2017. Diagnosis and Treatment of Leishmaniasis: Clinical Practice Guidelines by the Infectious Diseases Society of America (IDSA) and the American Society of Tropical Medicine and Hygiene (ASTMH). Am J Trop Med Hyg 96:24–45.
20. Guery R, Henry B, Martin-Blondel G, Rouzaud C, Cordoliani F, Harms G, Gangneux J-P, Foulet F, Bourrat E, Baccard M, Morizot G, Consigny P-H, Berry A, Blum J, Lortholary O, Buffet P. 2017. Liposomal amphotericin B in travelers with cutaneous and muco-cutaneous leishmaniasis: Not a panacea. PLoS Negl Trop Dis 11.
21. Wijnant G-J, Van Bocxlaer K, Yardley V, Harris A, Murdan S, Croft SL. 2018. Relation between Skin Pharmacokinetics and Efficacy in AmBisome Treatment of Murine Cutaneous Leishmaniasis. Antimicrob Agents Chemother 62.
22. Felton T, Troke PF, Hope WW. 2014. Tissue Penetration of Antifungal Agents. Clin Microbiol Rev 27:68–88.
23. Ternant D, Ducourau E, Perdriger A, Corondan A, Le Goff B, Devauchelle-Pensec V, Solau-Gervais E, Watier H, Goupille P, Paintaud G, Mulleman D. 2014. Relationship between inflammation and infliximab pharmacokinetics in rheumatoid arthritis. Br J Clin Pharmacol 78:118–128.

24. Slaviero KA, Clarke SJ, Rivory LP. 2003. Inflammatory response: an unrecognised source of variability in the pharmacokinetics and pharmacodynamics of cancer chemotherapy. Lancet Oncol 4:224–232.
25. Wu NZ, Da D, Rudoll TL, Needham D, Whorton AR, Dewhirst MW. 1993. Increased microvascular permeability contributes to preferential accumulation of Stealth liposomes in tumor tissue. Cancer Res 53:3765–3770.
26. Poh S, Chelvam V, Low PS. 2015. Comparison of nanoparticle penetration into solid tumors and sites of inflammation: studies using targeted and nontargeted liposomes. Nanomedicine (Lond) 10:1439–1449.
27. Blot SI, Pea F, Lipman J. 2014. The effect of pathophysiology on pharmacokinetics in the critically ill patient--concepts appraised by the example of antimicrobial agents. Adv Drug Deliv Rev 77:3–11.
28. Sykes EA, Dai Q, Tsoi KM, Hwang DM, Chan WCW. 2014. Nanoparticle exposure in animals can be visualized in the skin and analyzed via skin biopsy. Nat Commun 5:3796.
29. Mehta RT, McQueen TJ, Keyhani A, López-Berestein G. 1994. Phagocyte Transport as Mechanism for Enhanced Therapeutic Activity of Liposomal Amphotericin B. CHE 40:256–264.
30. Girard AE, Cimochowski CR, Faiella JA. 1996. Correlation of increased azithromycin concentrations with phagocyte infiltration into sites of localized infection. J Antimicrob Chemother 37 Suppl C:9–19.
31. Drusano GL. 2005. Infection site concentrations: their therapeutic importance and the macrolide and macrolide-like class of antibiotics. Pharmacotherapy 25:150S-158S.
32. Kelly C, Jefferies C, Cryan S-A. 2011. Targeted Liposomal Drug Delivery to Monocytes and Macrophages. J Drug Deliv 2011.
33. Voak AA, Harris A, Qaiser Z, Croft SL, Seifert K. 2017. Pharmacodynamics and Biodistribution of Single-Dose Liposomal Amphotericin B at Different Stages of Experimental Visceral Leishmaniasis. Antimicrob Agents Chemother 61.
34. Lasic DD, Papahadjopoulos D. 1995. Liposomes revisited. Science 267:1275–1276.
35. Radu M, Chernoff J. 2013. An in vivo assay to test blood vessel permeability. J Vis Exp e50062.

36. Nidavani RB, Am M, Shalawadi M. 2014. Vascular permeability and Evans blue dye: a physiological and pharmacological approach -. Journal of Applied Pharmaceutical Science 4:106–113.
37. krzyzanowska agi, Martin Y, Avendaño C, Piedras MJ, Krzyzanowska A. 2010. Evaluation of Evans Blue extravasation as a measure of peripheral inflammation. Protocol Exchange.
38. Fehrenbacher JC, Vasko MR, Duarte DB. 2012. Models of Inflammation: Carrageenan- or Complete Freund's Adjuvant-Induced Edema and Hypersensitivity in the Rat. Curr Protoc Pharmacol 0 5:Unit5.4.
39. Morris CJ. 2003. Carrageenan-induced paw edema in the rat and mouse. Methods Mol Biol 225:115–121.
40. Wijnant G-J, Van Bocxlaer K, Yardley V, Murdan S, Croft SL. 2017. Efficacy of Paromomycin-Chloroquine Combination Therapy in Experimental Cutaneous Leishmaniasis. Antimicrob Agents Chemother 61.
41. Brajtburg J, Bolard J. 1996. Carrier effects on biological activity of amphotericin B. Clin Microbiol Rev 9:512–531.
42. Lestner JM, Howard SJ, Goodwin J, Gregson L, Majithiya J, Walsh TJ, Jensen GM, Hope WW. 2010. Pharmacokinetics and Pharmacodynamics of Amphotericin B Deoxycholate, Liposomal Amphotericin B, and Amphotericin B Lipid Complex in an In Vitro Model of Invasive Pulmonary Aspergillosis. Antimicrob Agents Chemother 54:3432–3441.
43. Lopez-Berestein G, Rosenblum MG, Mehta R. 1984. Altered tissue distribution of amphotericin B by liposomal encapsulation: comparison of normal mice to mice infected with Candida albicans. Cancer Drug Deliv 1:199–205.
44. Alexander J, Kaye PM. 1985. Immunoregulatory pathways in murine leishmaniasis: different regulatory control during Leishmania mexicana mexicana and Leishmania major infections. Clin Exp Immunol 61:674–682.
45. El-On J, Lang E, Kuperman O, Avinoach I. 1989. Leishmania major: histopathological responses before and after topical treatment in experimental animals. Exp Parasitol 68:144–154.

46. Clay GM, Valadares DG, Graff JW, Ulland TK, Davis RE, Scorza BM, Zhanbolat BS, Chen Y, Sutterwala FS, Wilson ME. 2017. An Anti-Inflammatory Role for NLRP10 in Murine Cutaneous Leishmaniasis. J Immunol 199:2823–2833.
47. Andrade-Narvaez FJ, Medina-Peralta S, Vargas-Gonzalez A, Canto-Lara SB, Estrada-Parra S. 2005. The histopathology of cutaneous leishmaniasis due to Leishmania (Leishmania) mexicana in the Yucatan peninsula, Mexico. Rev Inst Med Trop Sao Paulo 47:191–194.
48. Dainichi T, Hanakawa S, Kabashima K. 2014. Classification of inflammatory skin diseases: A proposal based on the disorders of the three-layered defense systems, barrier, innate immunity and acquired immunity. Journal of Dermatological Science 76:81–89.
49. Oja CD, Semple SC, Chonn A, Cullis PR. 1996. Influence of dose on liposome clearance: critical role of blood proteins. Biochimica et Biophysica Acta (BBA) - Biomembranes 1281:31–37.
50. Varricchi G, Granata F, Loffredo S, Genovese A, Marone G. 2015. Angiogenesis and lymphangiogenesis in inflammatory skin disorders. J Am Acad Dermatol 73:144–153.
51. Bekersky I, Fielding RM, Dressler DE, Lee JW, Buell DN, Walsh TJ. 2002. Pharmacokinetics, Excretion, and Mass Balance of Liposomal Amphotericin B (AmBisome) and Amphotericin B Deoxycholate in Humans. Antimicrob Agents Chemother 46:828–833.
52. Wijnant GJ, Van Bocxlaer K, Yardley V, Harris A, Alavijeh M, Silva-Pedrosa R, Antunes S, Mauricio I, Murdan S, Croft SL. 2018. Comparative efficacy, toxicity and biodistribution of the liposomal amphotericin B formulations Fungisome and AmBisome in murine cutaneous leishmaniasis. Submitted to International Journal of Parasitology, under review.
53. Kloehn J, Saunders EC, O'Callaghan S, Dagley MJ, McConville MJ. 2015. Characterization of Metabolically Quiescent Leishmania Parasites in Murine Lesions Using Heavy Water Labeling. PLOS Pathogens 11:e1004683.
54. Mandell MA, Beverley SM. 2017. Continual renewal and replication of persistent Leishmania major parasites in concomitantly immune hosts. PNAS 114:E801–E810.
55. Jara M, Berg M, Caljon G, de Muylder G, Cuypers B, Castillo D, Maes I, Orozco M del C, Vanaerschot M, Dujardin J-C, Arevalo J. 2017. Macromolecular biosynthetic parameters and metabolic profile in different life stages of Leishmania braziliensis: Amastigotes as a functionally less active stage. PLoS One 12.

56. Zhao M, Lepak AJ, Andes DR. 2016. Animal models in the pharmacokinetic/pharmacodynamic evaluation of antimicrobial agents. Bioorg Med Chem 24:6390–6400.
57. von Stebut E. 2007. Cutaneous Leishmania infection: progress in pathogenesis research and experimental therapy. Exp Dermatol 16:340–346.
58. Mears ER, Modabber F, Don R, Johnson GE. 2015. A Review: The Current In Vivo Models for the Discovery and Utility of New Anti-leishmanial Drugs Targeting Cutaneous Leishmaniasis. PLoS Negl Trop Dis 9:e0003889.
59. McCormick TS, Stevens SR, Kang K. 2000. Macrophages and cutaneous inflammation. Nature Biotechnology 18:25.
60. Pasparakis M, Haase I, Nestle FO. 2014. Mechanisms regulating skin immunity and inflammation. Nat Rev Immunol 14:289–301.
61. Gutiérrez V, Seabra AB, Reguera RM, Khandare J, Calderón M. 2016. New approaches from nanomedicine for treating leishmaniasis. Chem Soc Rev 45:152–168.
62. Antonio L de F, Fagundes A, Oliveira RVC, Pinto PG, Bedoya-Pacheco SJ, Vasconcellos E de CF e, Valete-Rosalino MC, Lyra MR, Passos SRL, Pimentel MIF, Schubach A de O. 2014. Montenegro skin test and age of skin lesion as predictors of treatment failure in cutaneous leishmaniasis. Rev Inst Med Trop Sao Paulo 56:375–380.
63. Machado P, Araújo C, Silva D, T A, Almeida RP, D'Oliveira A, Bittencourt A, Carvalho EM. 2002. Failure of Early Treatment of Cutaneous Leishmaniasis in Preventing the Development of an Ulcer. Clin Infect Dis 34:e69–e73.
64. Van Bocxlaer K, Yardley V, Murdan S, Croft SL. 2016. Drug permeation and barrier damage in Leishmania-infected mouse skin. J Antimicrob Chemother 71:1578–1585.
65. Van Bocxlaer K, Gaukel E, Hauser D, Park SH, Schock S, Yardley V, Randolph R, Plattner JJ, Merchant T, Croft SL, Jacobs RT, Wring SA. 2018. Topical Treatment for Cutaneous Leishmaniasis: Dermato-Pharmacokinetic Lead Optimization of Benzoxaboroles. Antimicrob Agents Chemother 62.

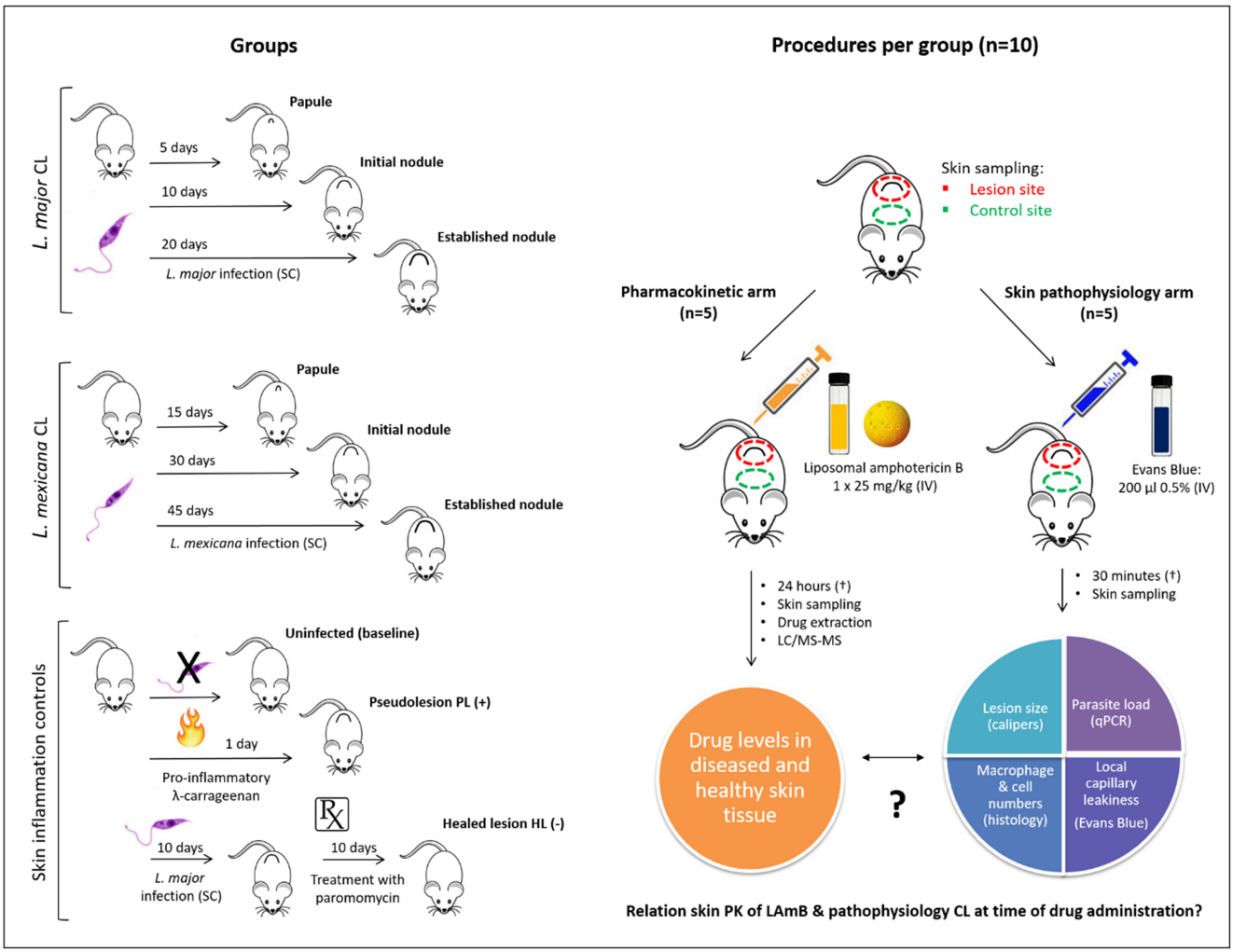

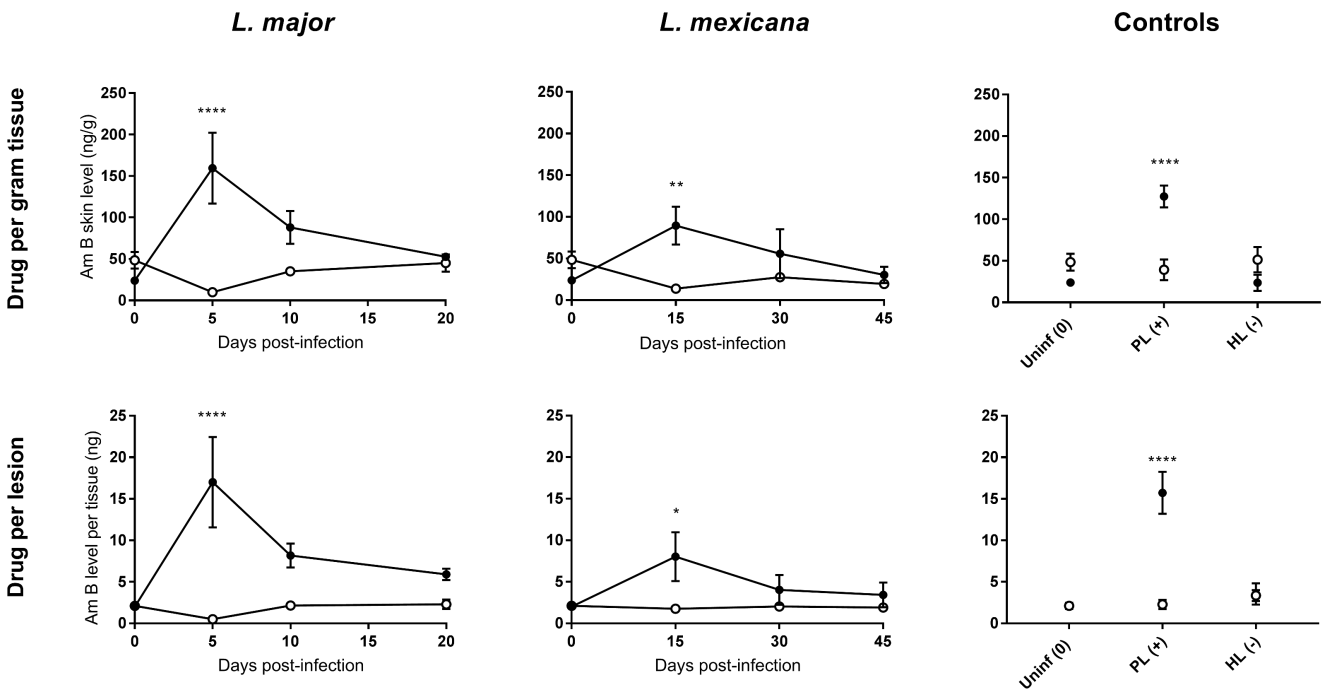

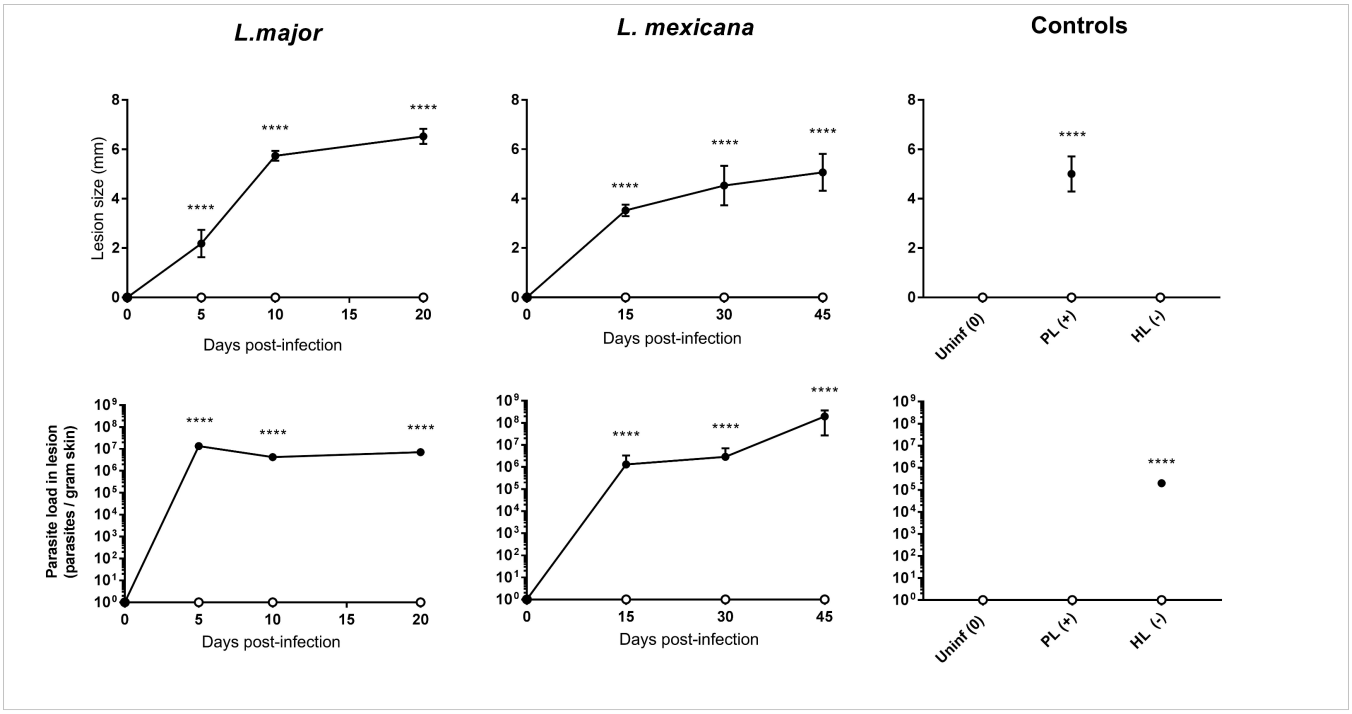

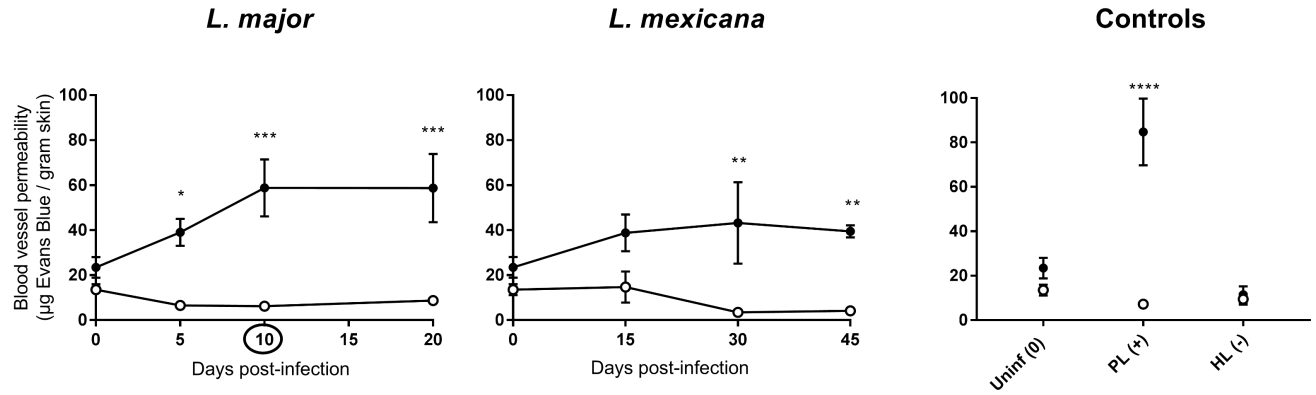

Evans Blue treated *L. major*-infected mice (day 10 post-infection):

Before skin sample collection

After skin sample collection

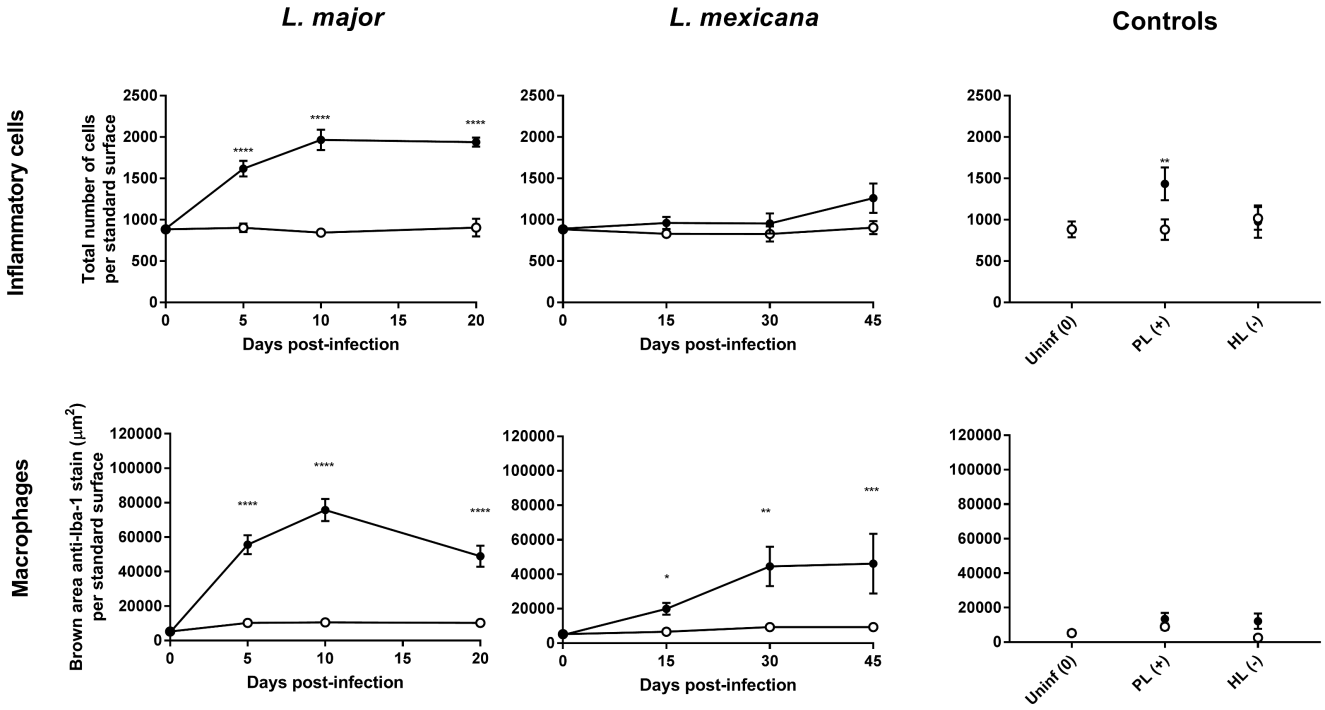

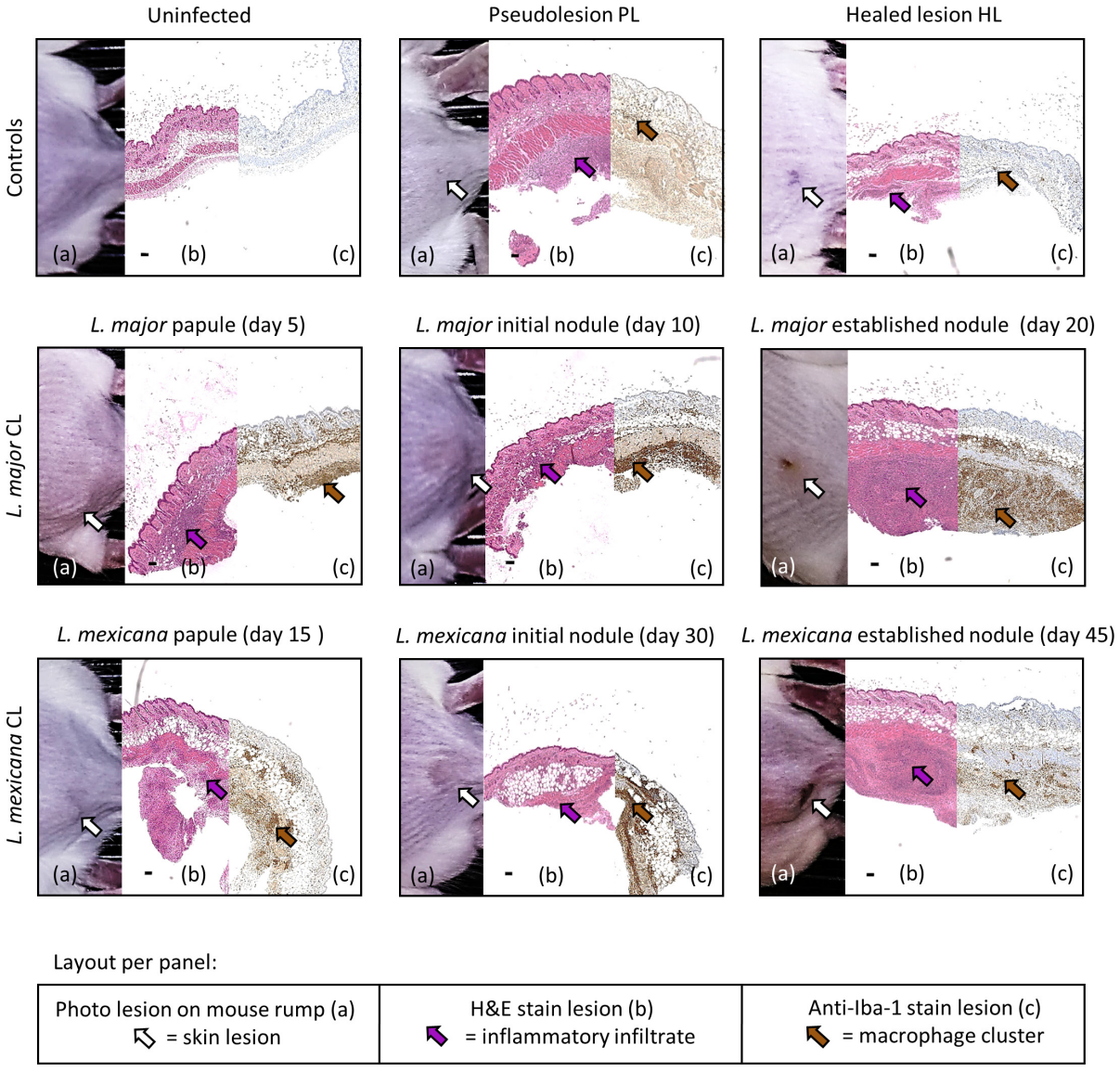

Healthy, uninfected skin

L. major lesion

L. mexicana lesion